Supporting Information

Hydrophilic Silver Nanoparticles Induce Selective Nanochannels in Thin Film Nanocomposite Polyamide Membranes

Zhe Yang,[a] Hao Guo,[a] Zhi-kan Yao,[a] Ying Mei[a] and Chuyang Y. Tang[a,b,c*]

[a] Department of Civil Engineering, the University of Hong Kong, Pokfulam, Hong Kong

[b] UNESCO Centre for Membrane Science and Technology, School of Chemical Engineering, University of New South Wales, Sydney, New South Wales 2052, Australia

[c] UNSW Water Research Centre, School of Civil and Environmental Engineering, University of New South Wales, Sydney, New South Wales 2052, Australia

[*] To whom all correspondence should be addressed.

Tel: +852 2859 1976, Fax: +852 2559 5337, E-mail address: tangc@hku.hk

This SI contains16 pages, with 10 figures and 1 table.

Table of Contents

32 **S1. SEM micrographs, silver mass density, contact angles and permeability of**

33 **the control and AgNPs modified PSF substrates**

34 The control PSF showed flat surface (Figure S1). With the increased concentration of

35 $NaBH_4$ and $CuSO_4$, increasing amounts of fine particles appeared on the PSF surface

36 and subsequently the substrate pore size decreased. These nanoparticles are AgNPs

37 based on the reaction between NaBH4 and $AgNO_3$.[1] The PSF-Ag substrate with

38 AgNPs coating became more hydrophilic compared to the control PSF.

39

40 To determine the total amounts of silver in the AgNPs incorported TFN membranes,

41 the membrane coupon (Membrane area = 1 cm^2) was immersed in a HNO_3 solution

42 (0.2 ml 69% HNO_3 dissolved in 20 ml DI water) shaking under 100 rpm for 3 days.

43 The dissolved silver concentrations leached in the HNO_3 solutions were also

44 determined by ICP. Figure S1 shows significantly increased silver loading at higher

45 $AgNO_3$.

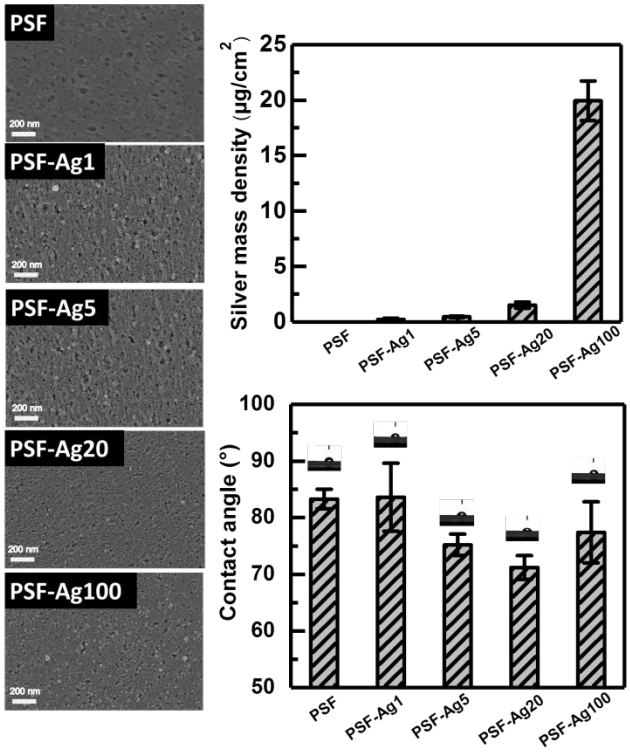

Figure S1. SEM surface micrographs, AgNPs mass density, and contact angle results of the control PSF and AgNPs modified PSF.

Figure S2 shows the water permeability of the control PSF and PSF-Ag substrates. The water permeability of the substrate was not significantly affected when AgNPs loading was relatively low (e.g., PSF-Ag1,5,20). Even at the highest silver loading, the PSF-Ag100 substrate showed only approximately 10% flux reduction compared to the control PSF.

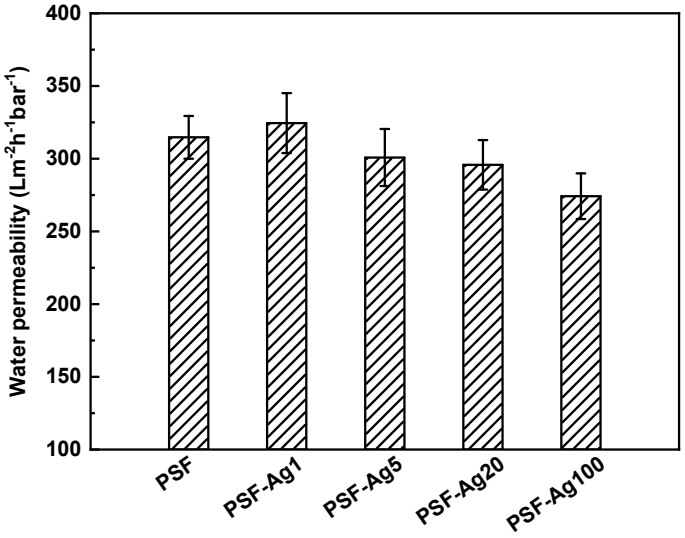

55

56 Figure S2. Water permeability of the control PSF and AgNPs modified PSF substrates

57

58 **S2. Size distributions of the AgNPs induced nanochannels**

59 Figure S3 shows the size distribution of the nanochannels in the vicinity of each

60 AgNPs. Their size of approximately 2.5 nm is nearly independent on the AgNPs

61 loading.

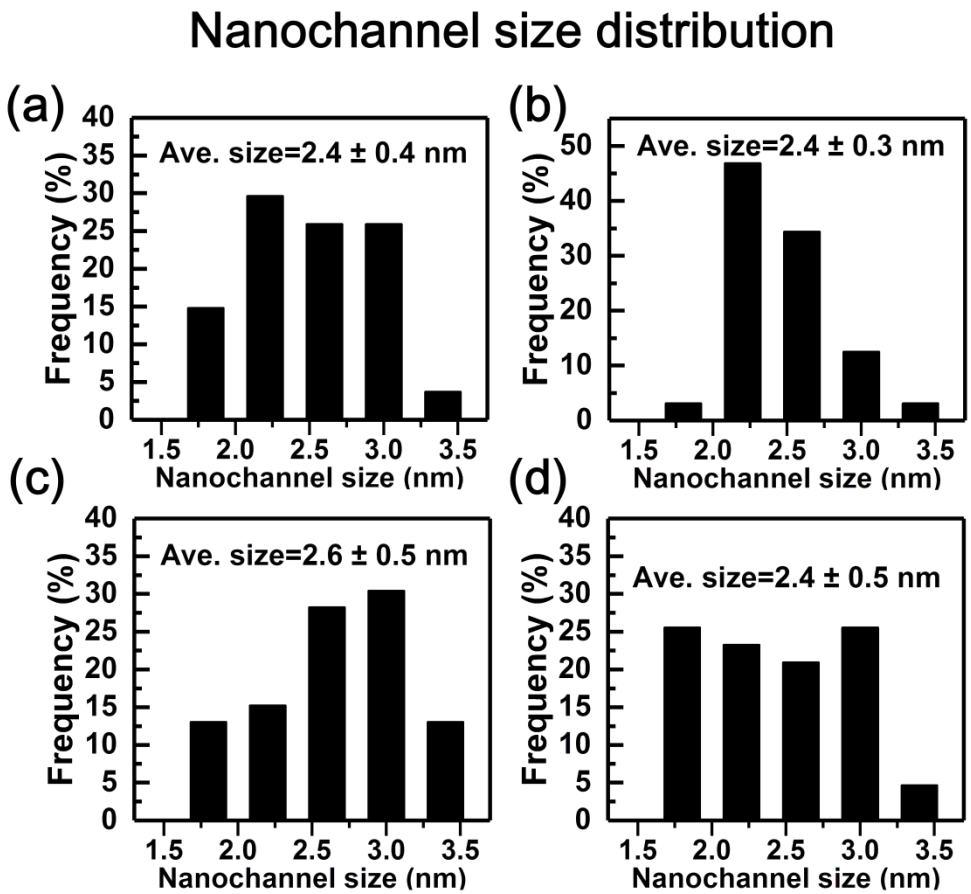

62

63 Figure S3. Size distribution of the nanochannels of silver nanoparticles in (a) TFC-Ag1, (b)

64 TFC-Ag5, (c) TFC-Ag20 and (d) TFC-Ag100 membranes.

65

66

S3. Physiochemical properties of TFC membranes

Figure S4 presents the contact angle results of all membranes. With the exception of TFC-Ag1 (within experimental variations), the other TFC-Ag membranes showed slightly decreased contact angles, thanks to the hydrophilicity of the AgNPs.

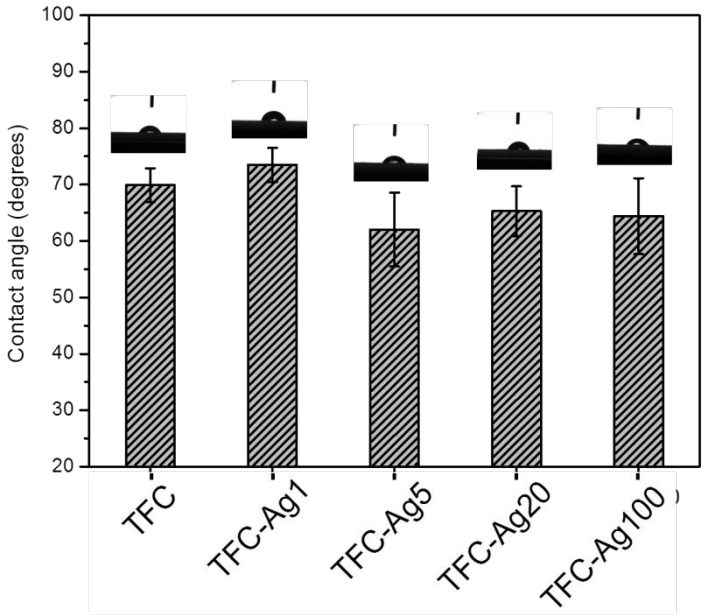

Figure S4. Contact angle results of all membrane.

FTIR results (Figure S5) show the characteristic peaks at 1541 cm^{-1} (the Amide II band), 1609 cm^{-1} (aromatic N-H deformation vibration) and 1663 cm^{-1} (the Amide I band), confirming the formation of polyamide chemistry formed by *m*-phenylenediamine (MPD) and trimesoyl chloride (TMC).[2]

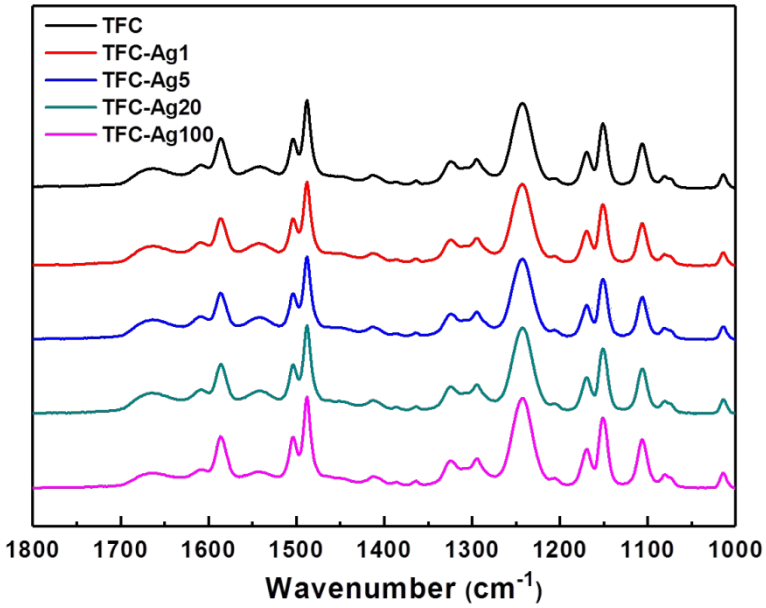

Figure S5. ATR-FTIR results of all membranes.

The elemental content of the polyamide rejection layers was determined by XPS. Since the AgNPs were covered by polyamide, the Ag peak cannot be detected at typical silver loading (e.g., TFC-Ag20, see Figure 4b in the main text) due to the low penetration depth of XPS. Figure S6 shows the XPS spectrum of TFC-Ag100 membrane. The Ag peak was identified for this membrane, which was likely caused by the aggregation of AgNPs under this high AgNP loading.

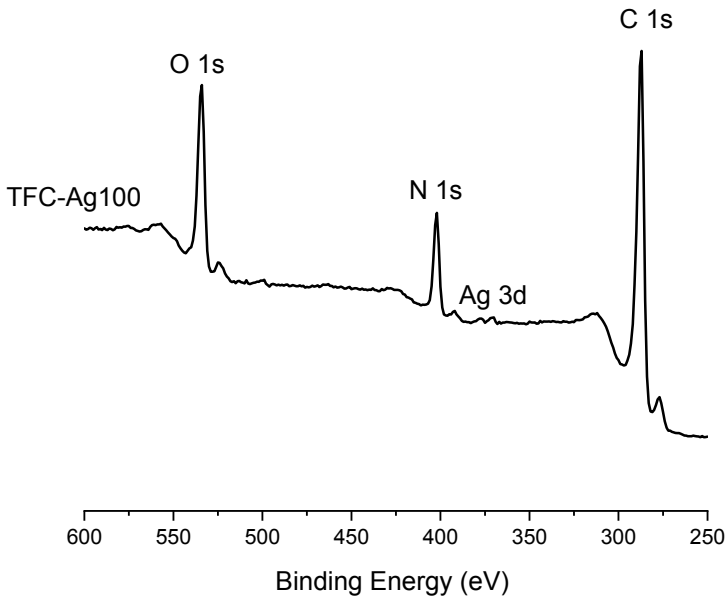

Figure S6. XPS spectrum of TFC-Ag100 membrane.

Figure S7 shows the high resolution TEM cross-sections of the TFC-Ag20 membrane (obtained by FEI Tecnai G2 20 Scanning TEM). In Figure S7a, AgNPs were typical present in individual particles with minimum aggregation. The corresponding magnified image (Figure S7b) shows the presence of nanochannels around the AgNPs.

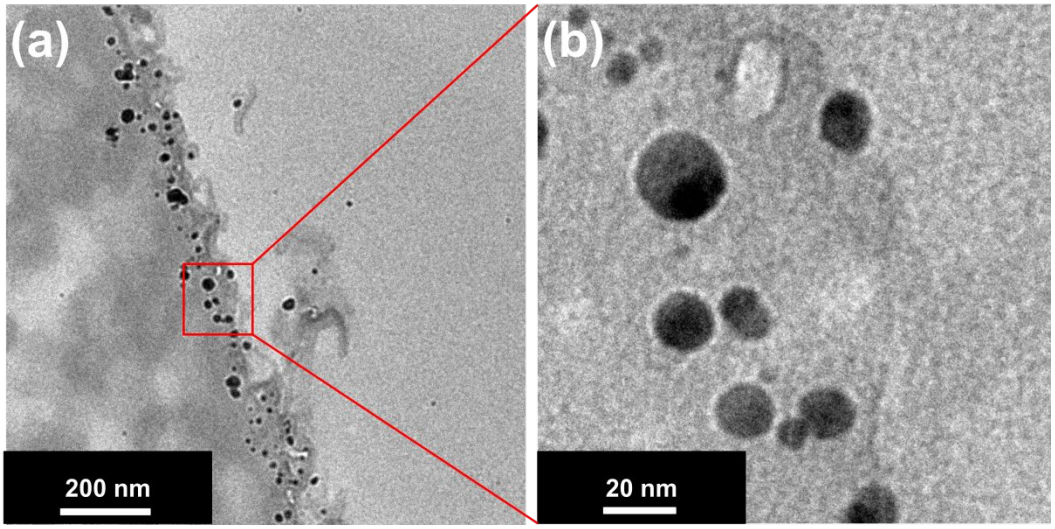

Figure. S7. High solution TEM cross-sections of the TFC-Ag20 membrane.

101 **S4. Zeta potential of AgNPs**

102 Surface zeta potential of AgNPs were measured using the zeta analyzer (ZEN3600,
103 Malven Ltd. UK). AgNPs solution (100 mg/L in deionized water) with pH adjusted at
104 6 or 7 was used for the determination of zeta potential. Table S1 shows that AgNPs
105 are negatively charged with zeta potential of -31.2 ± 0.2 and -32.1 ± 0.5 at testing pH
106 of 6 and 7.

107

108 Table S1. Zeta potential of AgNPs

100 mg/L zeta potential (mV)	pH=6	pH=7
AgNPs	-31.2 ± 0.2	-32.1 ± 0.5

109

110

S5. Calculation of Debye length

The Debye length can be calculated by Equation S1:[3]

$$\lambda_D = \frac{3.043 \times 10^{-10}}{\sqrt{I}} \tag{S1}$$

where λ_D is the Debye length (m) and I is the ionic strength (M). With a feed NaCl concentration of 2000 ppm and assuming a rejection of ~99%, the permeate concentration is ~ 20 ppm (0.00034 M), which corresponds to a Debye length of approximately 16.5 nm. Even if a much high NaCl concentration of 0.0034 M is used (with a NaCl rejection of 90%), the Debye length is still as large as 5.2 nm, which is approximately twice of the average size of the AgNP induced nanochannels.

S6. Calculation of membrane crosslinking degree

The crosslinking degree of a polyamide membrane can be determined from its O/N ratio. Figure S8 shows a polyamide chemical structure with both crosslinked (n) and linear ($1 - n$) fractions. The O/N ratio ($r_{O/N}$) can be calculated based on this chemical structure, and its value is 1 for $n = 1$ (fully crosslinking) and 2 for $n = 0$ (fully linear):

$$\frac{O}{N} = \frac{3n + 4(1-n)}{3n + 2(1-n)} \tag{S2}$$

Therefore, the crosslinking degree (n) can be determined once O/N ratio is measured:

$$n = \frac{4 - 2r_{O/N}}{1 + r_{O/N}} \tag{S3}$$

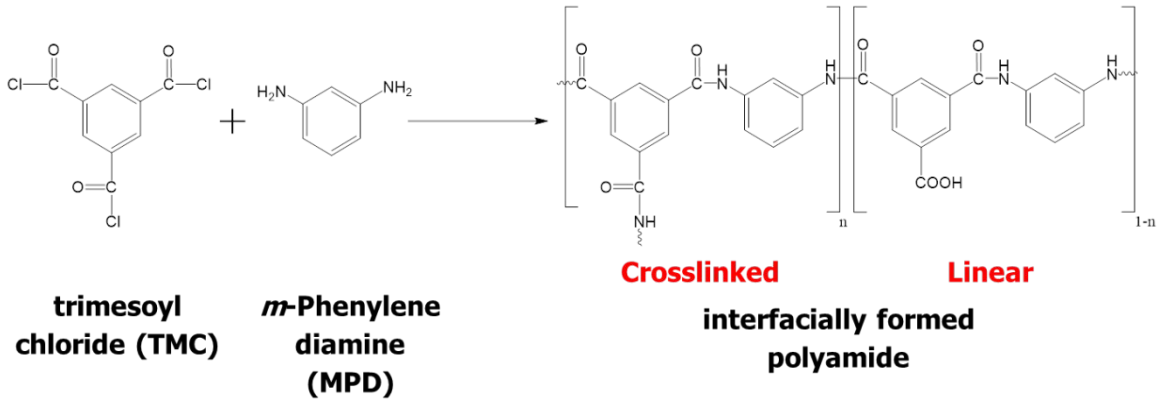

Figure S8. Interfacial polymerization reaction and chemical structure of polyamide.

S7. Membrane rejection of neutral hydrophilic solutes

Figure S9 presents the removal of neutral solutes (e.g., boron, ethylene glycol, diethylene glycol and pentaerythritol) by the TFC-Ag20 membranes. In general, the rejection improved compared to the control TFC. Two commercial RO membranes, i.e., BW30 and SW30HR, were also included as benchmarks for comparison. The solutes rejection of TFC-Ag20 membrane is higher than that of the brackish water RO membrane BW30 and was nearly comparable to that of the seawater RO membrane SW30HR.

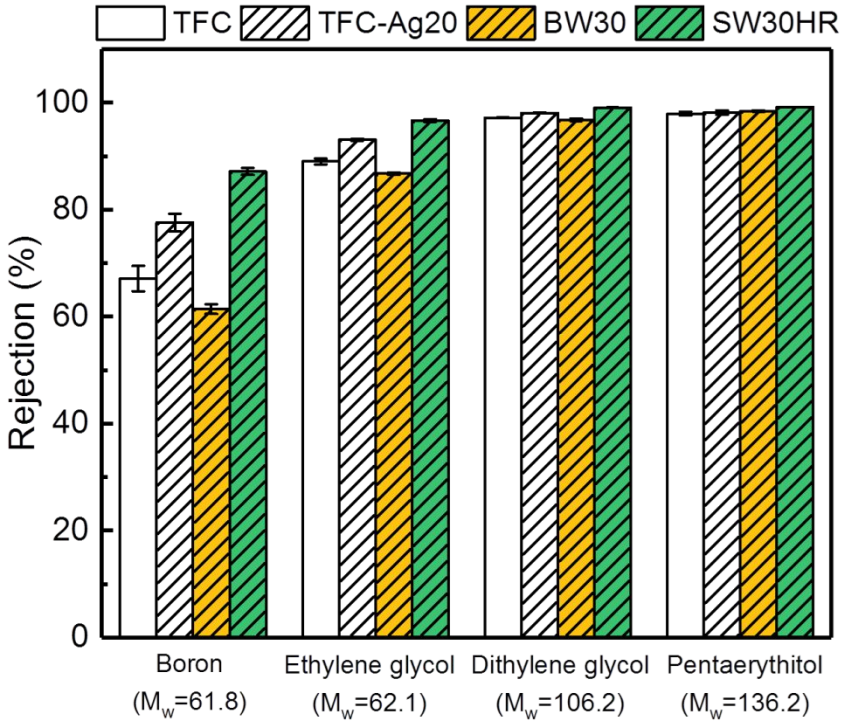

Figure S9. Neutral solutes rejection of the control TFC, TFC-Ag20 and two commercial RO membranes (BW30 and SW30HR).

S8. Membrane fouling behavior

Fouling tests were performed for the TFC control membrane and the TFC-Ag20 membrane using a feed water containing 20 ppm humic acid, 2000 ppm NaCl and 1 mM $CaCl_2$ (Figure S10). Since membrane fouling is highly sensitive to flux, an identical initial water flux of 17 $Lm^{-2}h^{-1}$ was applied for both membranes to ensure the fouling results can be directly compared. In the current study, the TFC-Ag20 membrane was able to maintain a more stable flux compared to the TFC control membrane. The enhanced antifouling property of the TFC-Ag20 membrane can be explained by its enhanced crosslinking degree with fewer surfaces $–COO^-$ groups to participate the membrane-Ca^{2+}-foulants bridging.[4]

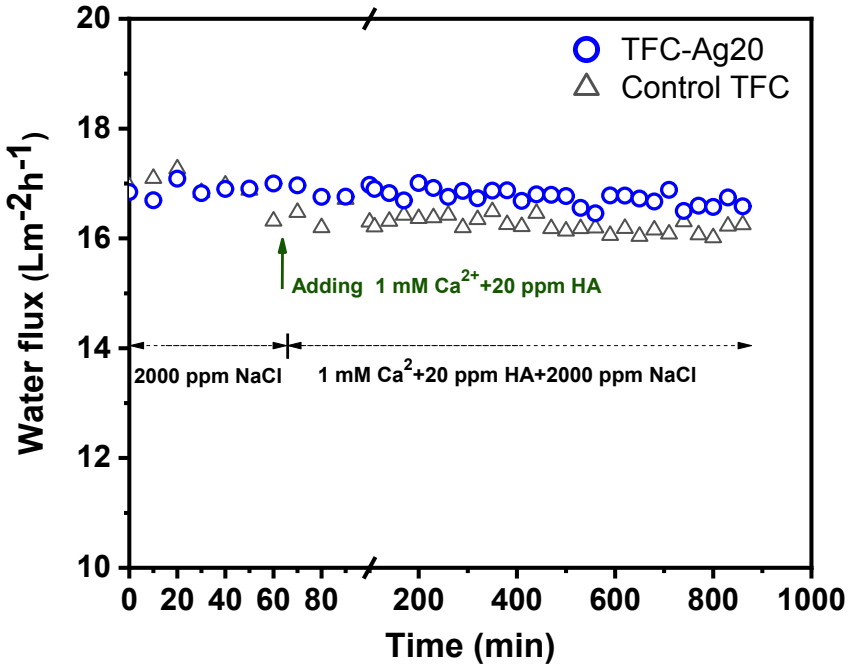

Figure S10. Membrane fouling tests by humic acid. Both membranes were pre-compacted at an applied pressure of 20 bar using a 2000 ppm NaCl solution as feed solution (pH 6.8, cross-flow velocity at 22.4 cm/s, and temperature at 25°C). Subsequently, the applied pressure was adjusted to achieve an initial flux of 17 $Lm^{-2}h^{-1}$ for both membranes. To start the fouling tests, humic acid (20 ppm) and $CaCl_2$ (1 mM) were added into the feed solution. The fouling tests were continued for 12 h.

References

1. Ben-Sasson, M.; Lu, X.; Bar-Zeev, E.; Zodrow, K. R.; Nejati, S.; Qi, G.; Giannelis, E. P.; Elimelech, M., In situ formation of silver nanoparticles on thin-film composite reverse osmosis membranes for biofouling mitigation. *Water Res.* **2014,** *62*, 260-70.

2. Tang, C. Y.; Kwon, Y.-N.; Leckie, J. O., Effect of membrane chemistry and coating layer on physiochemical properties of thin film composite polyamide RO and NF membranes: I. FTIR and XPS characterization of polyamide and coating layer chemistry. *Desalination* **2009,** *242*, (1-3), 149-167.

3. Tang, C. Y.; Kwon, Y.-N.; Leckie, J. O., The role of foulant–foulant electrostatic interaction on limiting flux for RO and NF membranes during humic acid fouling—Theoretical basis, experimental evidence, and AFM interaction force measurement. *J. Membr. Sci.* **2009,** *326*, (2), 526-532.

4. Tang, C. Y.; Kwon, Y.-N.; Leckie, J. O., Fouling of reverse osmosis and nanofiltration membranes by humic acid—effects of solution composition and hydrodynamic conditions. *J. Membr. Sci.* **2007,** *290*, (1-2), 86-94.